JOURNAL OF SPACECRAFT AND ROCKETS
Vol. 36, No. 3, May–June 1999

Aerodynamics of Stardust Sample Return Capsule

R. A. Mitcheltree,* R. G. Wilmoth,* F. M. Cheatwood,† G. J. Brauckmann,* and F. A. Greene*
NASA Langley Research Center, Hampton, Virginia 23681

Successful return of interstellar dust and cometary material by the Stardust Sample Return Capsule requires an accurate description of the Earth entry vehicle's aerodynamics. This description must span the hypersonic-rarefied, hypersonic-continuum, supersonic, transonic, and subsonic flow regimes. Data from numerous sources are compiled to accomplish this objective. These include direct simulation Monte Carlo analyses, thermochemical nonequilibrium computational fluid dynamics, transonic computational fluid dynamics, existing wind-tunnel data, and new wind-tunnel data. Four observations are highlighted: 1) a static instability is revealed in the free-molecular and early transitional flow regimes due to aft location of the vehicle's center of gravity, 2) the aerodynamics across the hypersonic regime are compared with the Newtonian flow approximation and a correlation between the accuracy of the Newtonian flow assumption and the sonic line position is noted, 3) the primary effect of shape change due to ablation is shown to be a reduction in drag, and 4) a subsonic dynamic instability is revealed that necessitated the addition of a stabilizing drogue parachute.

Nomenclature

C_A = axial force coefficient
C_m = moment coefficient
C_N = normal force coefficient
D = base diameter of capsule, m
Kn = Knudsen number
M = Mach number
P = pressure, N/m^2
R = radius of curvature, m
s = distance from stagnation point, m
t = independent variable time, s
V = velocity, m/s
$x_{c.g.}$ = location of center of gravity from nose, m
$x_{c.p.}$ = location of center of pressure from nose, m
α = angle of attack, deg

Introduction

STARDUST,[1] the fourth Discovery class mission, is scheduled for launch in February 1999. In addition to collecting interstellar dust, the robotic spacecraft will fly within 100 km of the comet Wild-2 nucleus and collect presolar cometary material from the coma parent-molecular zone. These materials will be returned to Earth for submicrometer-level analysis. To accomplish the mission's objective, a capsule containing the collected particles must safely transit an intense Earth entry, descent, and landing. This paper focuses on the aerodynamics of the Stardust Sample Return Capsule (SRC) during that entry. The results also have relevance to other proposed sample return missions.

The entry of the Stardust SRC at 12.6 km/s will be the fastest Earth entry ever attempted. Its trajectory traverses the hypersonic-rarefied, hypersonic-continuum, supersonic, transonic, and subsonic flow regimes. The passive capsule, once released from its host bus, will rely solely on the predetermined balance between aerodynamic forces and gravity to guide it through those regimes to a parachute landing, within a 75-km ellipse, in the Utah Test Landing Range. High-fidelity aerodynamic knowledge is essential for mission success. The drag coefficient must be accurately described within each flight regime so that the cumulative effect of the deceleration results in a landing within the targeted Utah site. In addition, the capsule should possess sufficient aerodynamic stability to minimize angle-of-attack excursions during the severe heating portion of the trajectory. This stability must persist through the transonic and subsonic regimes to maintain a controlled attitude at parachute deployment.

The objective of this paper is to describe the aerodynamics of the Stardust SRC and assess whether the requirements cited are met. The description must be constructed with sufficient breadth and detail to populate an aerodynamic database suitable for six-degree-of-freedom (DOF) trajectory simulations. Data from numerous sources are compiled. These include direct simulation Monte Carlo (DSMC) analysis to describe the rarefied flow in the transitional regime, thermochemical nonequilibrium computational fluid dynamics (CFD) for the hypersonic regime, CFD and existing wind-tunnel data in the supersonic and transonic regime, and finally, new subsonic static and dynamic wind-tunnel test data.

A description of the entry capsule's geometry is presented first. Discussion of the approach taken to describe the static aerodynamics in each flight regime is next, followed by comments on the dynamics. Detailed description of the aerodynamics through each of the flight regimes requires knowledge of the expected trajectory. Three-degree-of-freedom simulations were computed to satisfy this need. From this estimated trajectory, discrete points are chosen for the high-fidelity analysis.

SRC Geometry

The forebody geometry of the SRC is a 60-deg half-angle sphere–cone with nose radius equal to 0.2286 m, shoulder radius of 0.01905 m, and overall diameter of 0.8128 m. The afterbody shape is a 30-deg cone that terminates with a flat stern whose radius is 0.2116 m. The geometry is shown in Fig. 1. The forebody heat shield is made of phenolic-impregnated carbon ablator (PICA). Surface recession at the nose due to heating rates as high as 1200 W/cm^2 is estimated to be 0.01194 m (0.47 in.) and 0.006858 m (0.27 in.) at the shoulder. For aerodynamic considerations, this shape change due to ablation is assumed to result in a forebody that remains a 60-deg sphere–cone except the nose radius increases to 0.2405 m, shoulder radius increases to 0.02591 m, and overall diameter decreases to 0.7991 m. The ablative shape change impact on the aerodynamics is presented.

Low-Density Aerodynamics

The Stardust SRC is released from the host spacecraft 3–4 h prior to atmospheric interface. When the spin-stabilized capsule arrives at the outer reaches of the atmosphere, it will encounter widely

Presented as Paper 97-2304 at the AIAA 15th Applied Aerodynamics Conference, Atlanta, GA, June 23–25, 1997; received Jan. 10, 1998; revision received Aug. 15, 1998; accepted for publication Feb. 22, 1999.

*Aerospace Engineer, Aerothermodynamics Branch, Aero and Gas Dynamics Division. Senior Member AIAA.
†Aerospace Engineer, Vehicle Analysis Branch, Space Systems and Concepts Division. Member AIAA.

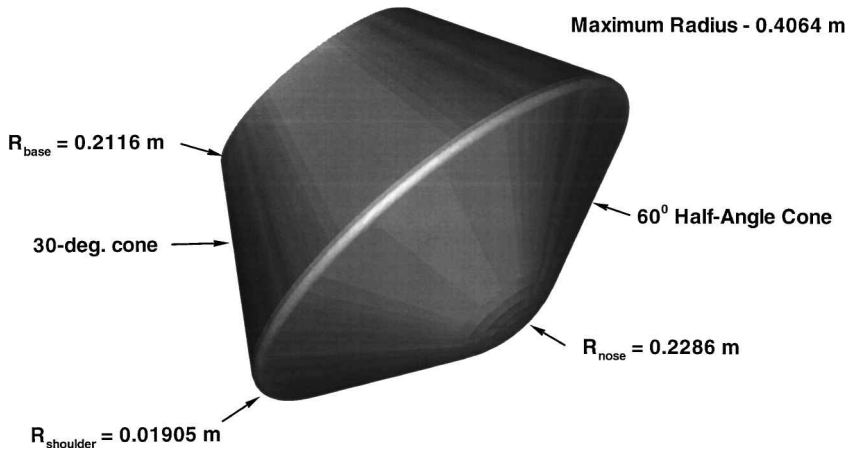

Fig. 1 Stardust SRC geometry.

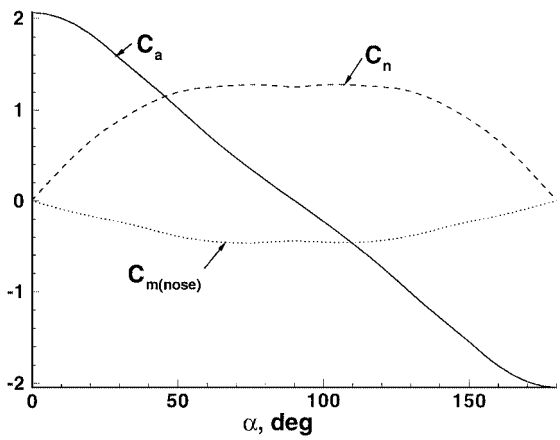

Fig. 2 Free-molecular flow aerodynamics.

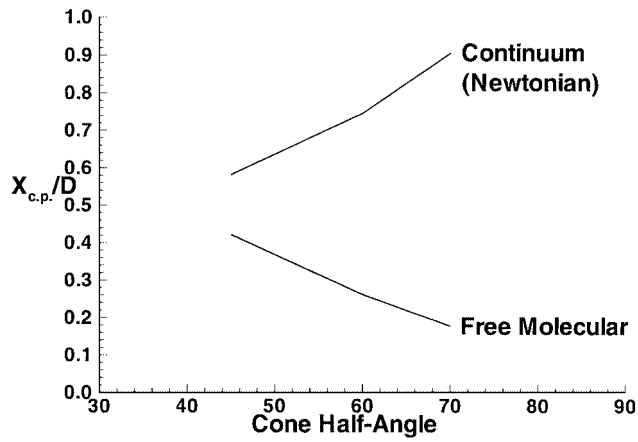

Fig. 3 Comparision of c.p. location for various cone half-angles.

spaced molecules. Surface impacts of these molecules will exert the first aerodynamic forces on the entry vehicle. Knudsen number Kn is defined as the ratio of the quiescent gas's mean free path to the vehicle's diameter. At the outer reaches of the atmosphere, Knudsen number is large. As long as $Kn > 10$, the associated aerodynamic forces can be accurately computed by a free-molecular flow method. Free-molecular flow assumes there are no collisions between gas molecules in the flowfield. The surface is impacted by freestream particles that are diffusely reflected after full thermal accommodation. Unlike hypersonic-continuum aerodynamics, where forces exerted on the blunt body are primarily the integrated effect of surface pressures, free-molecular flow aerodynamics contain a significant contribution from shear stress.

Free-molecular flow aerodynamics for the Stardust geometry are computed using a collisionless DSMC approach discussed in Ref. 2. The results are presented in Fig. 2. Because the geometry is axisymmetric, static aerodynamics can be described by the variation of axial force coefficient C_A, a normal force coefficient C_N, and a moment coefficient C_m with respect to angle of attack α. The reference area is the frontal area of the vehicle (0.51887 m^2), and the reference length is the diameter (0.8128 m). Unless otherwise specified, moments are taken about the nose of the vehicle.

As the capsule continues its descent to altitudes at or below 130 km, Knudsen number drops below 10 and collisions between molecules become important and must be included in aerodynamic predictions. This is the transitional flow regime. For a given Knudsen number, the transitional regime aerodynamics can be described by DSMC methods.[2–6] The low-density aerodynamics of the Stardust SRC is discussed in Ref. 2. A subset of the DSMC results is presented in Table 1.

Stardust (with its c.g. currently specified at $0.35D$) is unstable in the free-molecular flow region. It becomes stable about $\alpha = 0$ deg when Knudsen number drops below 0.09. The decrease in stability with increasing rarefaction, i.e., increasing Knudsen number, is a result of the increased shear stress contribution to the aerodynamic forces. This trend has been observed in Shuttle flights and documented for the blunt Soyuz capsule by Ivanov et al.[6] The divergence between continuum stability and free-molecular stability increases with bluntness, i.e., cone half-angle, as shown in Fig. 3.

The question arises as to whether the gyroscopic stability of the spinning capsule (originally at 5 rotations per minute) will be sufficient to retard the destabilizing aerodynamic forces until the capsule has passed through the altitudes at which the capsule is unstable.

The aerodynamic forces are proportional to the dynamic pressure. In the free-molecular flow regime, dynamic pressures are usually small because of low atmospheric densities. Stardust SRC, however, is smaller than past entry vehicles. Free-molecular and transitional flow conditions, therefore, persist to lower altitudes than previous vehicles experienced. Lower altitudes correspond to higher densities. In addition, the entry velocity at 12.6 km/s is higher than any other Earth entry. These two factors combine to result in non-negligible dynamic pressures (and thus aerodynamic forces) in the rarefied flow regimes. Furthermore, the interior of the capsule is somewhat empty so that its rotational inertia (and thus gyroscopic stability even at 5 rotations per minute) is small. Six-DOF calculations[7] indicate that the gyroscopic stability is not sufficient to retard the destabilizing aerodynamic forces. As a result, the capsule's angle of attack will increase from its desired 0-deg orientation toward a 60-deg trim point early in the trajectory. Large angles of incidence are worrisome because the capsule is stable flying backward. Off-nominal attitudes or pitch rates at atmospheric interface could result in a backward entry. In addition, large incidence angles early in the flight can result in incidence angles above 10 deg at peak heating. Large angles of attack dramatically increase the afterbody heating near the shoulder regions and may damage the afterbody thermal protection system.

Table 1 Three-dimensional results from DSMC (Ref. 5 method)

t, s	Alt, km	α	C_A	C_N	C_m
0	134.7	0	2.039	0	0
0	134.7	10	1.961	0.3294	−0.0875
0	134.7	30	1.541	0.8432	−0.2234
20	100.9	0	1.831	0	0
20	100.9	10	1.772	0.2330	−0.0738
20	100.9	30	1.403	0.5896	−0.2050
32	83.7	0	1.553	0	0
32	83.7	10	1.479	0.1244	−0.0505
32	83.7	30	1.097	0.3299	−0.1671

Table 2 Axisymmetric results from LAURA

t, s	Alt, km	M	V, m/s	C_A
32	83.7	42.7	12,592	1.5636
44	68.96	40	12,173	1.4959
53.2	58.7	35.4	10,983	1.4828
64	50.63	24.7	7,902	1.4816
72	46.54	17.1	5,496	1.4939
78	45.75	12.2	3,984	1.4992
82	44.44	10.5	3,289.0	1.515
86	43.24	8.5	2,724.5	1.510
92	41.60	7.15	2,076.2	1.506

Table 3 Three-dimensional results from LAURA

t, s	M	α	C_A	C_N	C_m
32	42.7	10	1.4807	0.10903	−0.05483
44	40.5	10	1.4455	0.08874	−0.06308
53.2	35.4	5	1.4740	0.04476	−0.03206
53.2	35.4	10	1.4338	0.08650	−0.06136
64.0	24.7	5	1.4708	0.04342	−0.03176
64.0	24.7	10	1.4303	0.08330	−0.05996
72	17.1	5	1.4806	0.04451	−0.03224
72	17.1	10	1.4208	0.07461	−0.05223
78	12.2	5	1.4889	0.04452	−0.03220
78	12.2	10	1.4242	0.07508	−0.05172
82	10.5	5	1.498	0.04074	−0.02822
86	8.5	5	1.496	0.03036	−0.01895
92	7.15	5	1.477	0.02270	−0.01309

Hypersonic Aerodynamics

As the capsule continues its descent below 66-km attitude, the Knudsen number drops below 0.001 and continuum methods can be used to describe the flow about (and the forces on) the capsule. In this hypersonic portion of the entry, the flowfield is dominated by a strong bow shock. Forebody pressures are two orders of magnitude larger than afterbody pressures. The afterbody can, therefore, be neglected when computing the aerodynamic characteristics at small angles of attack in this regime. The LAURA CFD code[8] is used to compute solutions at nine points in the trajectory's hypersonic regime. LAURA is an upwind-biased, point-implicit relaxation algorithm for obtaining the numerical solution to the Navier–Stokes equations for three-dimensional, viscous, hypersonic flows in thermochemical nonequilibrium.[9] It has been used to describe the aerodynamics of several blunt bodies including Mars Pathfinder.[10] Table 2 presents the 0-deg angle-of-attack C_A results. Three-dimensional solutions at 5- and 10-deg angle of attack are computed for the forebody at the nine trajectory points (Table 3).

With Mach numbers above 12 for continuum conditions 11-species thermochemical nonequilibrium effects are included. At and below Mach 12, the flow is assumed to be in chemical equilibrium. The axisymmetric solutions are computed on shock-aligned grids with 30 points along the forebody and 64 points normal to the surface. The cell Reynolds number for the first cell off the wall is unity. Three-dimensional solutions utilize an axis-singularity-free grid with a 58 × 26 cell surface definition. Confidence in these computational grids for accurately resolving surface pressures stems from previous experiences[11,12] on similar geometries.

Figure 4 presents the LAURA calculations for zero angle-of-attack axial coefficient. Little variation in the predicted values occurs

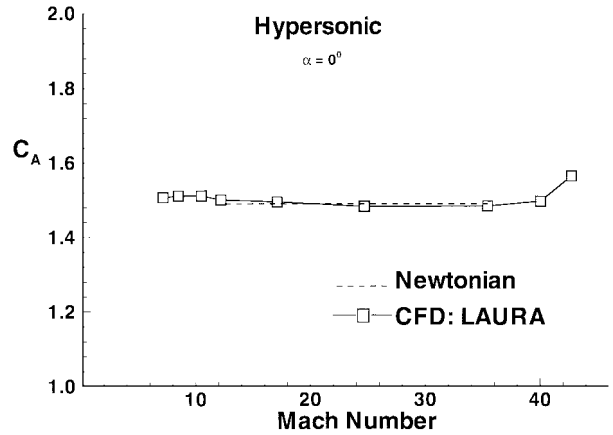

Fig. 4 Variation of axial force coefficients in the hypersonic flow regime.

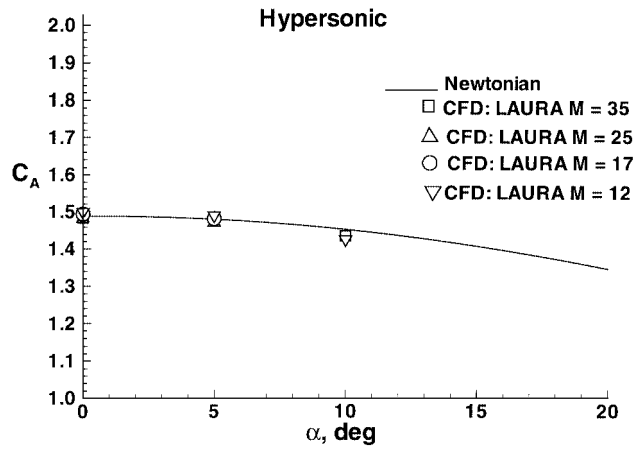

Fig. 5 Variation of axial force coefficient with angle of attack in the hypersonic flow regime.

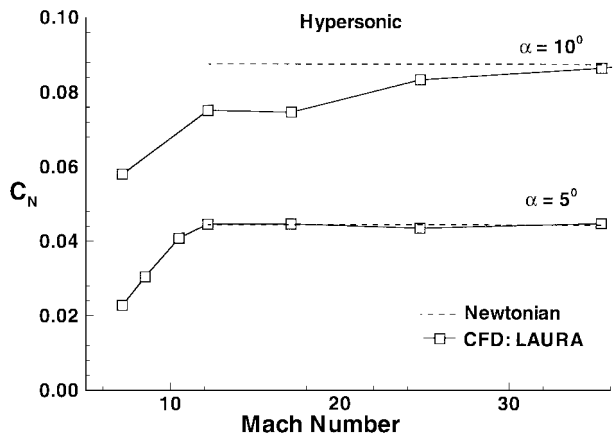

Fig. 6 Variation of normal force coefficients in the hypersonic flow regime.

across the entire hypersonic-continuum regime (above Mach 38 is the transitional regime where C_A increases toward its free-molecular value). A Newtonian flow prediction for the capsule is included as the dashed line. (Newtonian flow assumes that the freestream flow is turned parallel to the surface. Local pressure is then a function only of the local surface's inclination angle to the freestream.) Figure 5 presents the variation of the axial coefficient with angle of attack for CFD predictions above Mach 12. Increased angle of attack results in a small decrease in axial force across the Mach range.

Figures 6 and 7 display predicted normal-force and moment coefficients as a function of Mach number from 35 to 7 at 5- and 10-deg angle of attack. The marked decrease in normal force and

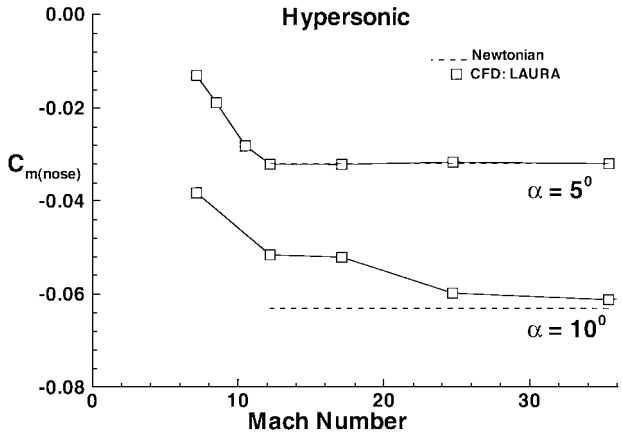

Fig. 7 Variation of moment coefficient in the hypersonic flow regime.

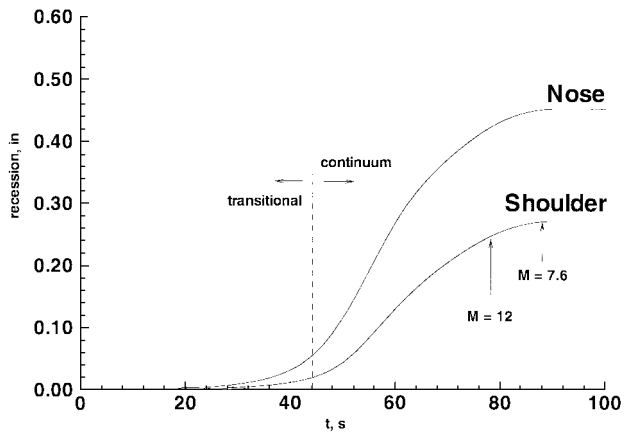

Fig. 8 Predicted surface recession during the entry trajectory.

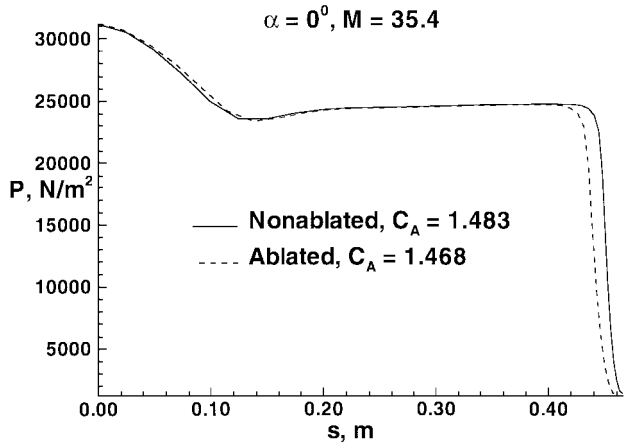

Fig. 9 Effect of surface recession on forebody pressures predictions.

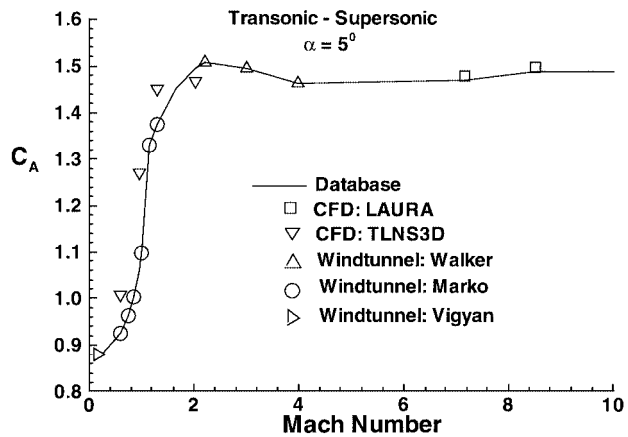

Fig. 10 Comparison of axial force coefficient predictions in the transonic and subsonic regimes.

increase in moment coefficients below Mach 12 is a result of the sonic line shifting from the sphere–cone tangency point to a location on the shoulder of the 60-deg forebody cone. This shift occurs as the flowfields exhibit less real-gas effects and begin to resemble ideal-gas flows. Pressure distributions (and thus aerodynamic forces) are affected by the sonic character of the shock layer. When supersonic, the pressure distributions on the conical flank are flat, which is characteristic of conical flow. When the entire forebody shock layer is subsonic, the elliptic nature of that flow results in higher, more rounded distributions. Figures 5–7 show that the Newtonian flow approximation is accurate only when the sonic line resides on the spherical nose. The net effect of the sonic line shift below Mach 12 is a decrease in the static stability margin [the center of pressure (c.p.) moves forward from $0.72D$ to $0.58D$ back from the nose].

The hypersonic regime aerodynamics are complicated by forebody shape change due to ablation. Thus far, the discussion of hypersonic aerodynamics has excluded this shape change. As the vehicle encounters heating as high as 1200 W/cm^2, the PICA forebody heatshield ablates and begins to recede. Figure 8 presents the predicted recession at the nose and the shoulder for the Stardust overshoot trajectory. Recession begins in the transitional flow regime and continues down to Mach 8. Surface recession decreases the frontal area, i.e., diameter, and increases the nose radius. Figure 8 supplied the information used to describe the ablated shape discussed in the "SRC Geometry" section. A LAURA solution is generated on the ablated shape (Mach 35.4). A comparison of forebody pressures and axial coefficients for the original and ablated geometry as predicted by LAURA is presented in Fig. 9. The shape change results in a decrease in axial coefficient of 0.8%. This change is primarily a result of the ablated shape's rounder shoulder. A Newtonian flow approximation of the ablated shape predicts a 0.6% decrease in the axial coefficient.

A comparison of the normal force and moment coefficients between the nonablated and ablated shape shows little change. These aerodynamic coefficients are, however, referenced to their respective areas, diameters, and nose locations. The total drag on the vehicle will decrease with ablation shape change more than the 0.8% indicated as a result of the decrease in reference area. In creating an aerodynamic database, these reference shifts must be tracked accurately.

Supersonic Aerodynamics

Below Mach 7, forebody-only CFD will not accurately predict the aerodynamics. The calculations must include the afterbody and wake. Such calculations are computationally expensive. Fortunately, wind-tunnel data for configurations similar to the SRC exist. In the low hypersonic and supersonic regions, Walker and Weaver[13] measured the static aerodynamics on blunted 60-deg cones in the Jet Propulsion Laboratory (JPL) 20-in. supersonic wind tunnel. The Reynolds number for these tests, based on diameter, is 4×10^6. (The expected flight Reynolds numbers in this speed regime are around 0.2×10^6.) The 60-deg sphere–cone models Walker and Weaver tested possessed a range of shoulder radii that envelopes the expected Stardust value. They performed measurements on a sharp-shouldered model and one with a shoulder radius equal to 5% of the base radius. The Stardust ablated geometry has a shoulder radius at 3.25% of its base radius. Unfortunately, the nose bluntness of their models (30% of the base radius) is not as large as the Stardust ablated geometry's (59% of the base radius) and the wind-tunnel models had no afterbody.

Figures 10–12 present C_A, C_N, and C_m as a function of Mach number for $\alpha = 5$ deg. (The transonic and subsonic data in the plots are discussed later.) In the supersonic regime, Figs. 10–12 indicate that little change in the aerodynamic coefficients occurs between Mach 7.15, where the last LAURA solution is generated, and Mach 4, where the Walker and Weaver data begins. Whereas Mach 3.98 is the highest value Walker and Weaver test for the models closest to

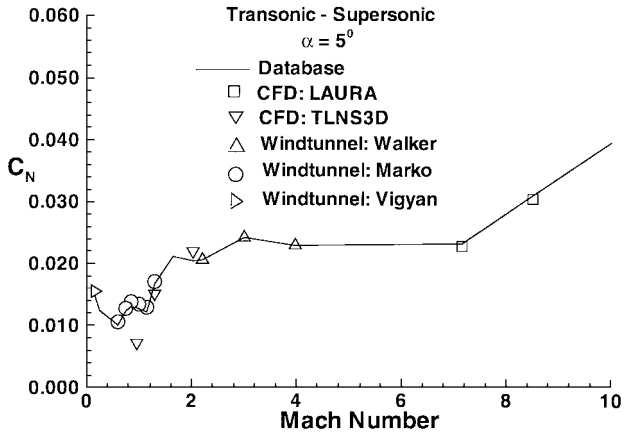

Fig. 11 Comparison of normal force coefficient predictions in the transonic and subsonic regimes.

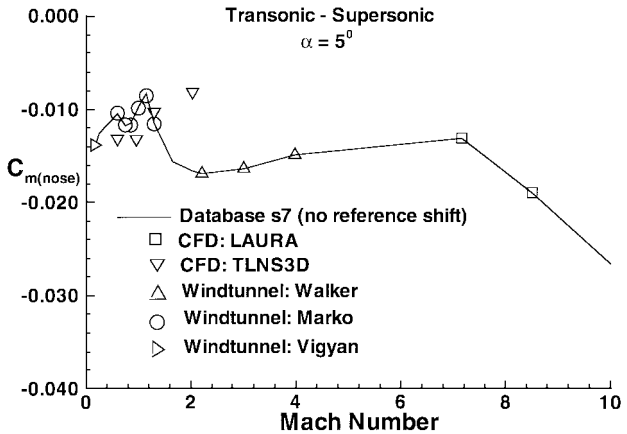

Fig. 12 Comparison of moment coefficient predictions in the transonic and subsonic regimes.

Stardust, they did examine similar 60-deg cones up to Mach 9.5 in the JPL 21-in. hypersonic wind tunnel. Their results show no change in the aerodynamics between Mach 9.5 and Mach 4. They also compared their Mach 9.5 results to modified Newtonian predictions and saw poor agreement. This observation agrees with earlier results displayed in Figs. 4–7, which revealed the Newtonian approximation to be accurate only down to Mach 12 where the sonic-line shift occurs. Note that the solid line in Figs. 10–12 labeled "database" is included to indicate trends.

Transonic Aerodynamics

Wind-tunnel measurements examining the same 60-deg wind tunnel models Walker and Weaver[13] examined at supersonic speeds were performed at transonic conditions by Marko,[14] in the NASA Ames Research Center 2 × 2 ft transonic wind tunnel. The data were measured at a Reynolds number based on diameter of 1×10^6; the flight value is near 0.2×10^6. These measurements are included in Figs. 10–12. Marko did not include the moment coefficient measurements in his report. He included c.p. locations at a subset of his test conditions, which, combined with the normal coefficient data, were used to compute the moment coefficients shown in Fig. 12. Windtunnel testing around Mach 1.0 is difficult due to reflected shock interference. Though Marko does not suggest this as a potential source of errors in his measurements, the data contain oscillations in C_N and C_m at Mach 1.0.

In an attempt to augment the definition of the transonic region aerodynamics, the CFD code TLNS3D[15] was used to examine the flight conditions between Mach 0.6 and 2.0. The results are included in Figs. 10–12. Some questions exist as to the accuracy of these CFD solutions. The concerns center around computation of the wake flow. The TLNS3D solver requires a turbulence model to be used to avoid numerical instabilities in the massive recirculation wake zone. However, none of the available turbulence models are accurate in such a separated flow region. Extensive grid resolution studies were performed, but questions remain as to the solution's accuracy. The largest question in the CFD predictions occurs in C_N, though not shown, the predicted value at $M = 0.6$ and $\alpha = 5$ deg is negative.

Subsonic Aerodynamics

The Stardust SRC entry scenario planned to deploy a parachute at 3-km altitude corresponding to a Mach number of 0.16. The deployment occurs 400 s after atmospheric interface. Of these 400 s of entry, 200 are spent at Mach numbers less than 0.6. The authors were not aware of any existing subsonic wind-tunnel data on the SRC shape. A wind-tunnel investigation of the Stardust SRC (0.30 scale ablated shape geometry) was conducted at Mach 0.16. The force and moment model of the SRC was constructed from high-density foam and covered with a fiberglass skin. Hard points within the structure were reinforced with aluminum and wood. The model was sting mounted to a six component balance through the base. The afterbody conical portion was fitted with six flush mounted pressure orifices in a longitudinal ray. (These pressure taps were incorporated to supply information necessary to calibrate the barometric parachute-deploy switch.)

The model was tested in the ViGYAN, Inc., low-speed wind tunnel in Hampton, Virginia. This tunnel is a conventional, straight-through, open-return-type layout with a 3 × 4 ft open-jet test section. The model was attached to an angle-of-attack mechanism, which was swept from 0- to 28-deg inclination. Balance data were reduced to coefficient form accounting for balance interactions, sting deflections, and model cavity pressures. The tunnel was run at a dynamic pressure of 0.018 atm. (The expected flight dynamic pressure is 0.012 atm.) Reynolds numbers based on diameter for the tests were 0.9×10^6. The resulting aerodynamic coefficients are listed in Table 4 and plotted in Figs. 13–15 as a function of angle of attack.

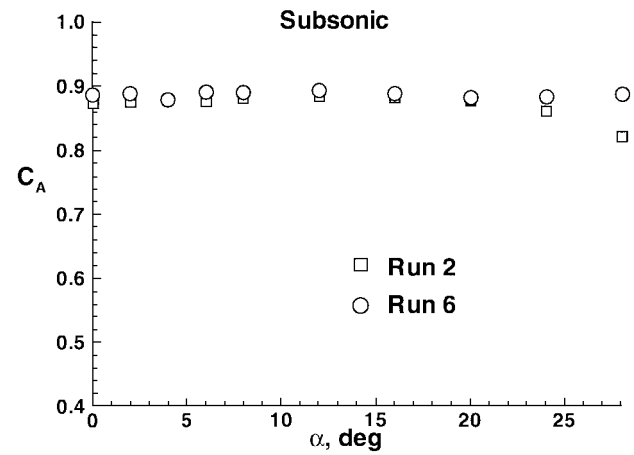

Fig. 13 Axial force coefficient measurements at subsonic conditions, $M = 0.16$.

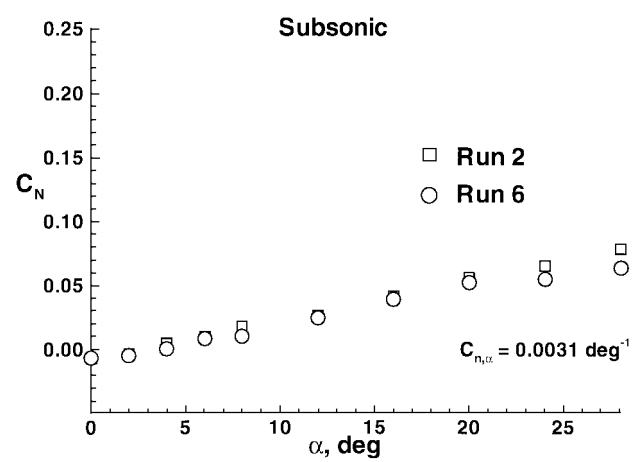

Fig. 14 Normal force coefficient measurements at subsonic conditions, $M = 0.16$.

Table 4 ViGYAN subsonic data ($M = 0.16$)

α	C_A	C_N	C_m
0.00	0.8739	0.0000	0.0000
2.02	0.8759	0.0053	−0.0058
4.00	0.8779	0.0119	−0.0115
6.04	0.8794	0.0177	−0.0171
7.99	0.8809	0.0242	−0.0227
12.02	0.8838	0.0357	−0.0332
16.01	0.8822	0.0485	−0.0446
20.00	0.8774	0.0613	−0.0573
24.01	0.8607	0.0723	−0.0676
28.01	0.8212	0.0855	−0.0757

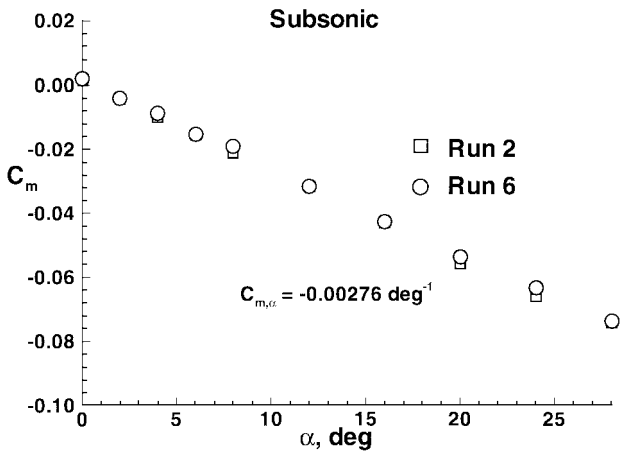

Fig. 15 Moment coefficient measurements at subsonic conditions, $M = 0.16$.

Note the normal force and moment coefficients may be considered linear over the angle-of-attack range examined. The data from these tests are also included at the far left-hand side of Figs. 10–12. The laminar or turbulent nature of the boundary layer for the flight case is not known, nor is it known whether the wind-tunnel test case was turbulent.

Dynamic Derivatives

Accurate six-DOF trajectory simulations of the SRC entry require knowledge of the dynamic stability of the capsule. This requirement is especially true in the transonic and subsonic speed regimes.

Uselton et al.[16] examined the dynamic stability of blunted 60- and 70-deg cones at Mach numbers between 3.0 and 0.6. They demonstrated that such shapes can suffer a dynamic instability at small angles of attack in the transonic flight regime. That is, though the shapes remain statically stable, when Mach number decreases below 2.0 an increase in incidence angles (a wobbling motion) may occur. Bendura[17] examined the dynamic stability of blunted 60-deg cones in the low subsonic regime and revealed a sensitive dependence on c.g. location. The desire for Stardust is that the capsule remain in a controlled flight through these speed regimes and that large oscillations do not exist at the Mach 0.16 parachute deployment.

Because the capsule spends the last 200 s of its entry at subsonic conditions, its attitude at parachute deploy is influenced most by its subsonic dynamic stability. To establish this property of the capsule, low subsonic dynamic stability tests were conducted in the 20-ft spin tunnel at NASA Langley Research Center. The tests revealed that the configuration was dynamically unstable at the conditions of the test due to the aft location of the c.g. ($0.35D$ back from the nose). Oscillations grew rapidly and diverged until the capsule began tumbling. If the c.g. was moved forward to $0.29D$, the divergent behavior was eliminated, and the capsule established itself in a limit-cycle oscillation with amplitude near 10 deg.

The addition of different sized drogue parachutes was examined as a means of stabilizing the original c.g. location configuration. A parachute with drag area of at least 0.208 m^2 was required to damp large perturbations. Details of these tests are discussed in Ref. 18.

At hypersonic speeds, ballistic-range-tests[19] do not discern significant changes in the values of the dynamic derivatives with Mach number. In addition, past experience with six-DOF simulations have also indicated that large variations in the dynamic derivatives at the higher Mach numbers have little effect on the hypersonic flight dynamics of the vehicle.

Conclusions

Successful return of interstellar dust and cometary material by the Stardust SRC requires an accurate description of the Earth entry vehicle's aerodynamics. This description must span the hypersonic-rarefied, hypersonic-continuum, supersonic, transonic, and subsonic flow regimes. Data from numerous sources are compiled. These sources include DSMC analyses, thermochemical nonequilibrium CFD, transonic CFD, existing wind-tunnel data, and new wind-tunnel data.

A static instability is revealed in the free-molecular and early transitional flow regime. The high entry velocity, small size, and low rotational inertia of the capsule combine to allow this instability the possibility of introducing large angles of attack during the high-altitude portion of the entry. Alleviation of the instability requires an increase in the spin rate from its original 5-rotations-per-minute specification to 16 rotations per minute.

In the hypersonic-continuum regime, CFD solutions reveal that the Newtonian flow assumption is reasonably accurate as long as the sonic line remains on the vehicle's spherical nose. This condition is true for angles of attack of 5 deg or less down to a Mach number of 12.

The sonic line shift from the spherical nose to the shoulder region below Mach 12 is accompanied by a forward movement of the c.p. ($0.72D$–$0.58D$), which decreases the static stability of the vehicle. This decrease in static stability is smaller than the one associated with the transition from continuum to free-molecular flow ($0.72D$–$0.26D$).

The primary effect of ablation shape change on the vehicle's aerodynamics is a decrease in the drag coefficient resulting from the rounding of the shoulders and decreased frontal area. Uncertainties in the degree of shape change will translate directly into uncertainties in the landing footprint.

Finally, a dynamic instability revealed in the subsonic regime will require the addition of a stabilizing drogue parachute with drag area at least 0.208 m^2. This parachute will be deployed at Mach 1.4.

Acknowledgments

Y. K. Chen of NASA Ames Research Center supplied the surface recession estimate. William Willcockson of Lockheed Martin Astronautics supplied the three-DOF estimated trajectory. Prasun Desai of NASA Langley Research Center (LaRC) was helpful in many discussions and performed six-DOF simulations, which revealed the static instability in the transitional flow regime. Thanks are also extended to J. N. Moss and D. F. Rault (LaRC) for supplying additional direct simulation Monte Carlo solutions and W. A. Wood (LaRC) for several LAURA computational fluid dynamics solutions.

References

[1] Willcockson, W. H., "Stardust Sample Return Capsule Design Experience," AIAA Paper 98-2854, June 1998.

[2] Wilmoth, R. G., and Mitcheltree, R. A., "Low-Density Aerodynamics of the Stardust Sample Return Capsule," AIAA Paper 97-2510, June 1997.

[3] Bird, G. A., "The G2/A3 Program User's Manual," G.A.B. Consulting Pty, Killara, Australia, March 1992.

[4] Rault, D. F., Cestero, F. J., and Shane, R. W., "Spacecraft Aerodynamic Characteristics During Aerobraking Maneuver in Planetary Atmospheres," AIAA Paper 96-1890, June 1996.

[5] Wilmoth, R. G., LeBeau, G. J., and Carlson, A. B., "DSMC Grid Methodologies for Computing Low-Density, Hypersonic Flows About Reusable Launch Vehicles," AIAA Paper 96-1812, June 1996.

[6] Ivanov, M. S., Markelov, G. N., Gimelshein, S. F., and Antonov, S. G., "DSMC Studies of High-Altitude Aerodynamics of Reentry capsule," *20th International Symposium on Rarefied Gas Dynamics*, edited by Ching Shen, Peking Univ. Press, Beijing, 1997, pp. 453–458.

[7] Desai, P. N., Mitcheltree, R. A., and Cheatwood, F. M., "Entry Dispersion Analysis for the Stardust Comet Sample Return Capsule," AIAA Paper 97-3812, Aug. 1997.

[8]Cheatwood, F. M., and Gnoffo, P. A., "User's Manual for the Langley Aerothermodynamic Upwind Relaxation Algorithm (LAURA)," NASA TM-4674, April 1996.

[9]Gnoffo, P. A., Gupta, R. N., and Shinn, J. L., "Conservation Equations and Physical Models for Hypersonic Air Flows in Thermal and Chemical Nonequilibrium," NASA TP-2867, Feb. 1989.

[10]Braun, R. D., Powell, R. W., Engelund, W. C., Gnoffo, P. A., Weilmuenster, K. J., and Mitcheltree, R. A., "Mars Pathfinder Six-Degree-of-Freedom Entry Analysis," *Journal of Spacecraft and Rockets*, Vol. 32, No. 6, 1995, pp. 993–1000.

[11]Gnoffo, P. A., "Computation of Near-Wake, Aerobrake Flowfields," *Journal of Spacecraft and Rockets*, Vol. 29, No. 2, 1992, pp. 182–189.

[12]Nettelhorst, H. L., and Mitcheltree, R. A., "Grid Resolution and Solution Convergence for Mars Pathfinder Forebody," NASA TM-1.09173, Dec. 1994.

[13]Walker, B., and Weaver, R. W., "Static Aerodynamic Characteristics of Blunted Cones in the Mach-Number Range from 2.2 to 9.5," Jet Propulsion Lab., TR-32-1213, California Inst. of Technology, Pasadena, CA, Dec. 1967.

[14]Marko, W. J., "Static Aerodynamic Characteristics of Three Blunted Sixty Degree Half-Angle Cones at Mach Numbers from 0.6 to 1.3," Jet Propulsion Lab., TR 32-1298, California Inst. of Technology, Pasadena, CA, July 1968.

[15]Vatsa, V. N., Turkel, E., and Abolhassani, J. S., "Extension of Multigrid Methodology to Supersonic/Hypersonic 3-D Viscous Flows," NASA CR-187612, Aug. 1991.

[16]Uselton, B. L., Shadow, T. O., and Mansfield, A. C., "Damping in Pitch Derivatives of 120 and 140 Deg Blunted Cones at Mach Numbers 0.6 Through 3.0," U.S. Air Force Arnold Engineering Development Center, TR-70-49, Arnold Air Force Station, TN, April 1970.

[17]Bendura, R. J., "Low Subsonic Static and Dynamic Stability Characteristics of Two Blunt 120 deg Cone Configurations," NASA TN-D-3853, Feb. 1967.

[18]Mitcheltree, R. A., and Fremaux, C. M., "Subsonic Dynamics of Stardust Sample Return Capsule," NASA TM-110329, March 1997.

[19]Krumins, M. V., "A Ballistic Range Study of the Aerodynamic Characteristics of Mars Probe/Lander Shapes," AIAA Paper 67-167, Jan. 1967.

R. D. Braun
Guest Editor